ISSN 0915-6364

NATIONAL INSTITUTE FOR FUSION SCIENCE

Low Energy Cross Section Data for Ion-molecule Reactions in Hydrogen Systems and for Carge Transfer of Multiply Charged Ions with Atoms and Molecules

K. Okuno

(Received - Feb. 13, 2007)

NIFS-DATA-100 Apr. 2007

RESEARCH REPORT
NIFS-DATA Series

TOKI, JAPAN

Low energy cross section data for ion-molecule reactions in hydrogen systems and for charge transfer of multiply charged ions with atoms and molecules

Kazuhiko Okuno

Tokyo Metropolitan University, Minami-ohsawa 1-1, Hachioji-shi, Tokyo 192-0397, Japan

Abstract

Systematic cross section measurements for ion-molecule reactions in hydrogen systems and for charge transfer of multiply charged ions in low energy collisions with atoms and molecules have been performed continuously by the identical apparatus installed with an octo-pole ion beam guide (OPIG) since 1980 till 2004. Recently, all of accumulated cross section data for a hundred collision systems has been entered into CMOL and CHART of the NIFS atomic and molecular numerical database together with some related cross section data. In this present paper, complicated ion-molecule reactions in hydrogen systems are revealed and the brief outlines of specific properties in low energy charge transfer collisions of multiply charged ions with atoms and molecules are introduced.

Keywords: ion-molecule reaction, charge transfer, multiply charged ions, single-electron capture, multiple-electron capture, cross section, electron beam ion source, ion beam guide, orbiting effects, Langevin cross section.

1. Introduction

In the last two decades, a great deal of atomic collision data, especially concerning on charge transfer of multiply charged ions in collisions with neutrals after development of ion source which can produce highly charged ions, have been accumulated. Cross section data for ion-molecule reactions in hydrogen systems and for charge transfer of multiply charged ions are not only considerable fundamentals on atomic physics but also quite important for fusion astrophysical plasma research. Especially the low energy data below 1 keV/amu are indispensable for diagnosis of fusion plasma, however they have been lacking still now because of technical difficulties in preparation of a stable ion beam with a narrow energy spread and in collection of large angle scattered ions.

In 1980, we constructed an tandem mass spectrometer with an octo-pole ion beam guide (OPIG) installed in collision chamber for the low energy collision experiments and first carried out cross section measurements for ion-molecule reactions in hydrogen systems to

Table 1. Lists of collision systems measured for cross section data.

(a). Ion-molecule reactions in hydrogen systems.

projectile	targets	projectile	targets	projectile	targets
$^{1}H^{+}$	H_2, D_2	$^{1}H_2^{+}$	H_2, D_2	$^{1}H_3^{+}$	H_2
$^{2}D^{+}$	H_2	$^{2}D_2^{+}$	H_2, D_2	$^{2}D_3^{+}$	H_2, D_2

(b). Collision systems for charge transfer of low-charged rare-gas ions with atoms and molecules.

projectile	targets	projectile	targets	projectile	targets
$^{20}Ne^{2+}$	He, H_2, N_2	$^{40}Ar^{2+}$	He, Ne, Ar, Kr	$^{84}Kr^{2+}$	He, Ne, Kr
		$^{40}Ar^{3+}$	He, Ne, Ar, Kr	$^{86}Kr^{3+}$	Kr

(c). Collision systems for charge transfer of multiply charged ions with atoms and molecules.

projectile	targets	projectile	targets	projectile	targets
$^{3}He^{2+}$	He, H_2, N_2, O_2, CO	$^{14}N^{6+}$	He, H_2	$^{40}Ar^{9+}$	He, Ne, H_2
$^{13}C^{2+}$	He, H_2	$^{16}O^{2+}$	He, H_2	$^{40}Ar^{11+}$	He, H_2
$^{13}C^{3+}$	He, H_2	$^{16}O^{3+}$	He, H_2	$^{86}Kr^{3+}$	CO
$^{12}C^{4+}$	He, Ne, Ar, Kr, H_2, N_2, O_2, CH_4, C_2H_6, C_3H_8, n-C_4H_{10}	$^{18}O^{4+}$	He, H_2	$^{84}Kr^{4+}$	CO
		$^{16}O^{5+}$	He, H_2	$^{84}Kr^{5+}$	CO
		$^{16}O^{6+}$	He, H_2	$^{84}Kr^{6+}$	CO
$^{12}C^{5+}$	He, H_2	$^{16}O^{7+}$	He	$^{84}Kr^{7+}$	Ne, CO
$^{13}C^{6+}$	He, H_2	$^{40}Ar^{4+}$	Ne	$^{84}Kr^{8+}$	Ne, N_2, O_2, CO
$^{14}N^{2+}$	He, H_2	$^{38}Ar^{5+}$	Ne	$^{84}Kr^{9+}$	Ne, CO
$^{14}N^{3+}$	He, H_2	$^{40}Ar^{6+}$	He, Ne, H_2	$^{127}I^{24+}$	He
$^{14}N^{4+}$	He, H_2	$^{40}Ar^{7+}$	He, Ne, H_2	$^{127}I^{25+}$	He
$^{14}N^{5+}$	He, H_2	$^{40}Ar^{8+}$	He, Ne, H_2	$^{127}I^{26+}$	He

inspect performance of the OPIG. The coaxial RF field oscillating in an enough high frequency proved to well confine ions on the axis of OPIG [1,2]. A small size electron beam ion source (Mini-EBIS) based on an idea of cooling magnetic solenoid coils with liquid nitrogen was developed in 1987 [3]. Since then the cross section measurements for the charge transfer of multiply charged ions have been performed systematically by combining both techniques of the OPIG and the Mini-EBIS [4]. Using the identical apparatus installed with an octo-pole ion beam guide (OPIG), low energy cross section data below 1keV/amu for a hundred collision systems listed in Table 1 have been measured and accumulated till now. Recently, all of them has been entered into CMOL and CHART of the NIFS atomic and molecular numerical database together with some related cross section data. Projectile ions of collision systems listed in Table 1 (a) and (b) were produced by the Nier type ion source (conventional electron impact type) and multiply charged ions in Table 1 (c) were extracted from the Mini-EBIS in the DC mode operation.

In this paper, the brief explanation of experimental technique used for low energy cross section measurements will be presented and the brief outlines of characteristics in low energy cross section data measured for ion-molecule reactions in hydrogen collision systems and for charge transfer of multiply charged ions in collisions with atoms and molecules will be introduced.

2. Experimental technique for low energy cross section measurements

The apparatus used for low energy cross section measurements is a tandem mass spectrometer consisted of an ion source, a mass selector, a collision cell, a mass analyzer and an ion detector in cascade. In the collision cell, the OPIG system composed of eight molybdenum poles is assembled in penetrating through the outlet of the cell. High frequency RF voltages are supplied to the eight poles of the OPIG alternatively in an opposite phase. The oscillatory electric field created in the OPIG modulates and confines only the radial motion of charged particles and never affect the drift motion along the axis. The OPIG is very powerful to prevent ion beam from diverging and to transport ion beam without its intensity loss.

At first a Nier type ion source of a conventional electron impact type was installed and it was displaced by the Mini-EBIS since 1987. In Fig.1, the experimental setup equipped with the Mini-EBIS is schematically illustrated together with a typical arrangement of electrostatic potentials. The collision energy was determined by the charge q times the potential difference ΔV between V_i at the ion source and V_c at the collision cell, so that

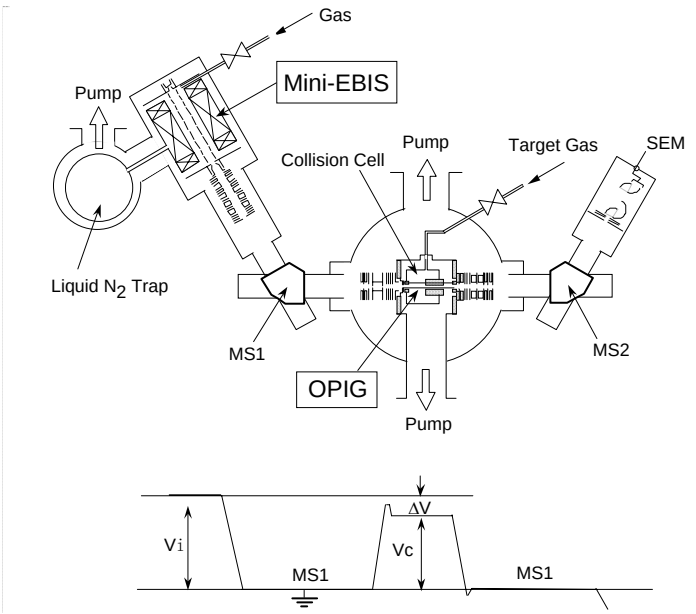

Fig.1. A schematic diagram of the experimental setup and the arrangement of electrostatic potentials.
Vacuum envelope is grounded. Vi and Vc are potentials at the ion source and the collision cell, respectively.

$E_{lab} = q \times \Delta V = q \times (V_i - V_c)$. When beam intensity was measured as a function of $\Delta V = V_i - V_c$, it was almost constant until it falls off rapidly near the zero energy as seen in Fig.2. This feature is of a great advantage of using the OPIG for the low energy cross section measurements. The Mini-EBIS was operated in the DC mode to eliminate energy spreads of the extracted ion beam. Energy spreads of the ion beam was estimated from a differential curve of the beam intensity, as typically $q \times 0.3$ eV (FWHM) for the Nier type ion source and $q \times (0.4\sim0.7)$ eV (FWHM) for the EBIS, respectively.

Cross sections for ion-molecule reactions and charge transfer were determined by the initial growth method with increasing the target gas pressure. The contamination of long-living excited ions in the ion beam often causes significant and dramatic effects on the cross section. Therefore, to check the contamination of long-living excited ions, we routinely measured attenuation cross sections of projectile ions in target gases.

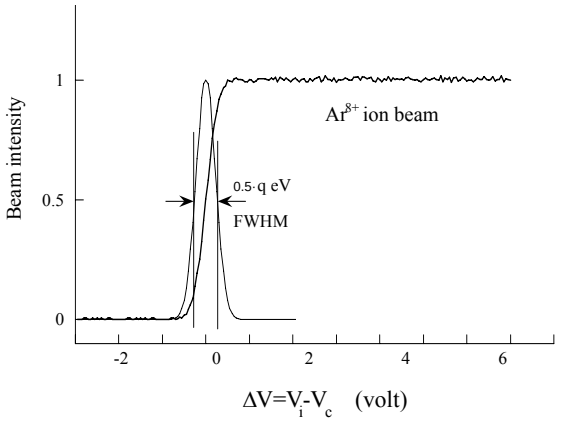

Fig.2. Intensity curve of Ar^{8+} beam extracted from the mini-EBIS as a function of the difference ($\Delta V = V_i - V_c$) between potentials at the ion source (V_i) and the collision cell (V_c).

3. Ion-molecule reactions in hydrogen systems

A tandem mass spectrometer can separate ions with different kinetic energies even if their masses are same. The tandem mass spectrometer installed an OPIG and a conventional Nier type ion source was first used in cross section measurements for ion-molecule reactions in hydrogen systems. In order to clearly resolve related reaction processes involving atomic rearrangement in such systems of H^+/H_2, H_2^+/H_2 and H_3^+/H_2, cross section measurements were carried out for various combination systems of isotopic species. Partial cross sections for every ion formation produced in $H^+(D^+)/H_2(D_2)$, $H_2^+(D_2^+)/H_2(D_2)$ and $H_3^+(D_3^+)/H_2(D_2)$ systems listed in Table 1(a) were measured together with σ(att) cross sections for beam attenuation of projectile ions in targets as a function of the collision energies from 0.1 to 1000 eV in the center-of-mass systems. From comparison among cross section data for isotope displaced systems, complicated ion-molecule reactions were successfully resolved in considerations of reaction energy and kinetic energy of product ions and it was imaged up that collisions were dominated by formation of an intermediate molecular complex at low energies below few eV in the center-of-mass systems and the molecular complex fragments resonantly one after another in the few eV energy region. This scheme informs us that atomic processes in hydrogen systems at low energies below 100 eV should be treated in the molecular base but not in the atomic base theoretically.

3.1. Ion-molecule reactions in the H^+/H_2 system

In order to resolve ion-molecule reactions in the H^+/H_2 system, related cross sections were measured for three collision systems of H^+/H_2, H^+/D_2 and D^+/H_2. The $\sigma(DH^+)$ cross section measured for DH^+ formation in the D^+/H_2 system involves contribution from some secondary H_3^+ formation processes of $H_2^+ + H_2 \rightarrow H_3^+ + H$. The pure $\sigma(DH^+)$ can be estimated by subtraction of secondary D_3^+ formation cross sections measured for the H^+/D_2 system instead of secondary H_3^+ formation cross sections. In hydrogen systems of the A^+/B_2 type, following five reaction processes (3-1)～(3-5) are proved to be conceivable. The reaction energy of each related channel slightly depends on isotope composition of the system due to small differences in dissociation and ionization energies of H_2, HD and D_2. Note that energy values of the five reaction processes are typically estimated with disregarding this isotope effect.

$$A^+ + B_2 \rightarrow AB + B^+ + 0\ eV \qquad \sigma(B^+) \qquad (3\text{-}1)$$

$$\rightarrow AB^+ + B - 1.83\ eV \qquad \sigma(AB^+) \qquad (3\text{-}2)$$

$$\rightarrow A + B_2^+ - 1.83\ eV \qquad \sigma(B_2^+) \qquad (3\text{-}3)$$

$$\rightarrow A + B + B^+ - 4.48\ eV \qquad \sigma(B^+) \qquad (3\text{-}4)$$

$$\rightarrow A^+ + B_2^+ + e - 15.43\ eV \qquad \sigma(B_2^+) \qquad (3\text{-}5)$$

In Fig.3, the resolved cross sections are demonstrated together with the attenuation cross sections of σ(att) and the Langevin cross section of σ_L. Especially for hydrogen systems of A^+/B_2 type, some secondary processes occur even in very thin target and there is large difference σ_Σ between σ(att) and sum of reaction cross sections measured. Also, there is possibility that momentum loss and/or large angle scattering in dominant reaction processes much reduces detection efficiency for product ions. All processes except for (3-1) are endothermic and their cross sections take a peculiar energy structure with a threshold related to reaction energy as seen in Fig.3.

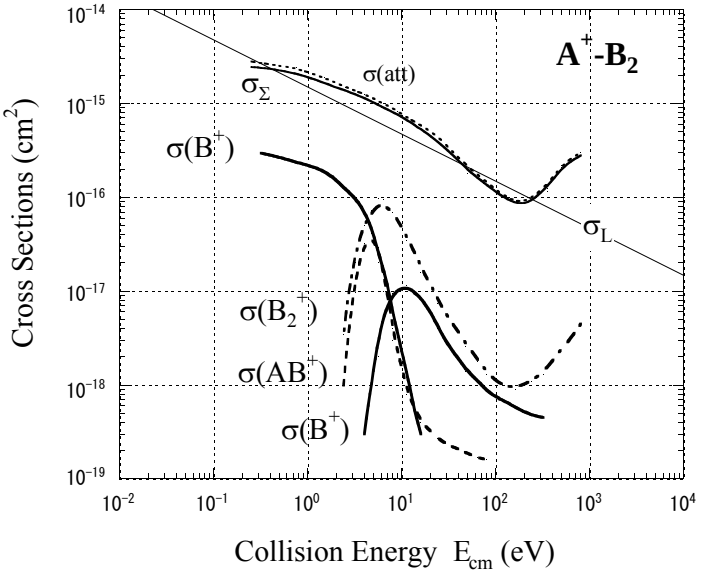

Fig. 3. Reaction cross sections in the A^+/B_2 type collision system

3.2. Ion-molecule reactions in the H_2^+ / H_2 system

In the type A_2^+/B_2 type collision systems in Table 1(a) where elements of A and B are H or D, six kinds of ion species of A_2B^+, AB_2^+, AB^+, A^+, B^+ and B_2^+ types were recognized. From comparison among reaction cross sections measured for product ions in the systems, following six reaction processes are resolved as are demonstrated in Fig.4.

$$A_2^+ + B_2 \rightarrow A_2B^+ + B + 2.06\ \text{eV} \qquad \sigma(A_2B^+) \qquad (3\text{-}6)$$

$$\rightarrow AB_2^+ + A + 2.06\ \text{eV} \qquad \sigma(AB_2^+) \qquad (3\text{-}7)$$

$$\rightarrow AB^+ + AB + 0\ \text{eV} \qquad \sigma(AB^+) \qquad (3\text{-}8)$$

$$\rightarrow A + A + B_2^+ - 4.47\ \text{eV} \qquad \sigma(B_2^+) \qquad (3\text{-}9)$$

$$\rightarrow A^+ + A + B_2 - 2.75\ \text{eV} \qquad \sigma(A^+) \qquad (3\text{-}10)$$

$$\rightarrow A_2 + B^+ + B - 2.75\ \text{eV} \qquad \sigma(B^+) \qquad (3\text{-}11)$$

$$\rightarrow A_2 + B_2^+ + 0\ \text{eV} \qquad \sigma_C(B_2^+) \qquad (3\text{-}12)$$

The ion-molecule reactions in the hydrogen systems of A_2^+/B_2 type are dominated by H_3^+ formation processes of (3-6) and (3-7) at low energies below 10 eV in the center-of-mass systems. A curve σ_Σ given by difference between σ(att) and total sum of cross sections measured for resolved processes of (3-7)~(3-10) should be shared mainly with cross sections of the symmetric resonant charge transfer process (3-12).

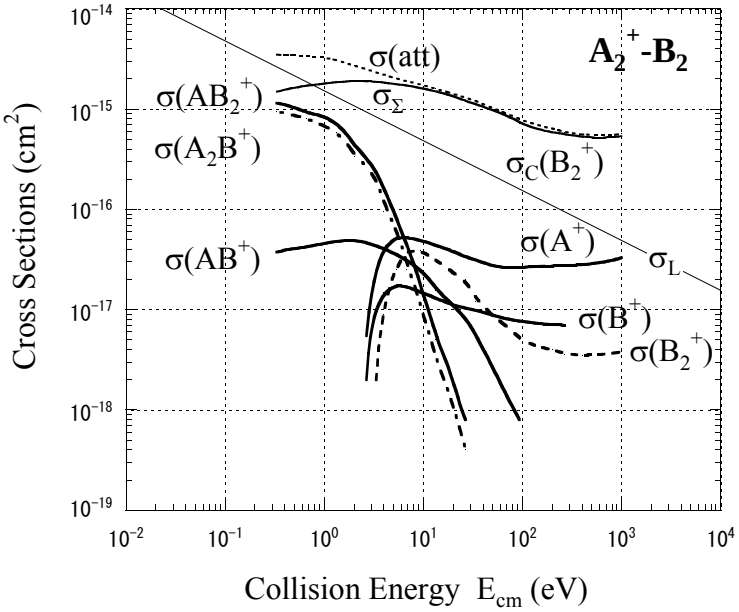

Fig.4. Reaction cross sections in the A_2^+/B_2 type collision system

3.3. Ion-molecule reactions in the H_3^+ / H_2 system

In the hydrogen systems of A_3^+/B_2 type, complicated ion-molecule reactions were supposed to be composed of following eleven reaction processes.

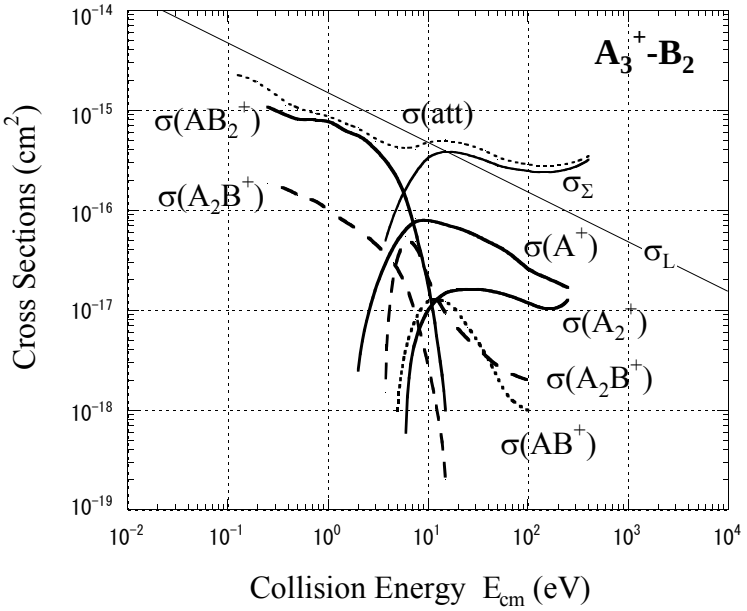

Fig.5. Reaction cross sections in the A_3^+/B_2 type collision system

$$A_3^+ + B_2 \rightarrow A_2B^+ + AB + 0\ eV \qquad \sigma(A_2B^+) \qquad (3\text{-}13)$$

$$\rightarrow A_2B^+ + A + B - 4.47\ eV \qquad \sigma(A_2B^+) \qquad (3\text{-}14)$$

$$\rightarrow AB_2^+ + A_2 + 0\ eV \qquad \sigma(AB_2^+) \qquad (3\text{-}15)$$

$$\rightarrow AB_2^+ + A + A - 4.47\ eV \qquad \sigma(AB_2^+) \qquad (3\text{-}16)$$

$$\rightarrow AB^+ + A_2 + B - 6.52\ eV \qquad \sigma(AB^+) \qquad (3\text{-}17)$$

$$\rightarrow AB^+ + AB + A - 6.52\ eV \qquad \sigma(AB^+) \qquad (3\text{-}18)$$

$$\rightarrow A^+ + A_2 + B_2 - 4.81\ eV \qquad \sigma(A^+) \qquad (3\text{-}19)$$

$$\rightarrow A_2^+ + A + B_2 - 6.52\ eV \qquad \sigma(A_2^+) \qquad (3\text{-}20)$$

$$\rightarrow A_2^+ + AB + B - 6.52\ eV \qquad \sigma(A_2^+) \qquad (3\text{-}21)$$

$$\rightarrow A_2 + AB + B^+ - 4.81\ eV \qquad \sigma(B^+) \qquad (3\text{-}22)$$

$$\rightarrow A_2 + A + B_2^+ - 6.52\ eV \qquad \sigma(B_2^+) \qquad (3\text{-}23)$$

Practically, while product ions of A_2B^+, AB_2^+, A^+ and A_2^+ types are observed, product ions of B^+ and B_2^+ types have been not recognized in measured systems of H_3^+/H_2, D_3^+/H_2 and D_3^+/D_2 listed in Table 1(a). By the isotope displacement technique, cross sections for reaction

processes of (3-13), (3-15), (3-17) and/or (3-18), (3-19), and (3-20) and/or (3-21) are resolved as shown in Fig.5.

In the A_3^+/B_2 type collision system, all processes except for (3-13) and (3-15) are endothermic. With increase of collision energy, dominant processes drastically exchange from processes of (3-13) and (3-15) to endothermic processes in the few eV energy region as seen in Fig.5. This situation is a phenomenon common throughout the hydrogen systems of A^+/B_2, A_2^+/B_2 and A_3^+/B_2. Although we have not observed B_2^+ product ions of (3-23) directly, it was proved experimentally that the slow B_2^+ product ion turn into the B_3^+ ion in a secondary process of $B_2^+ + B_2 \rightarrow B_3^+ + B$ during beam confinement time in the OPIG. Because energy dependence of apparent cross sections measured for formation of the secondary product ion of B_3^+ exactly likes to that of σ_Σ, σ_Σ might be contributed by the B_2^+ formation for the process (3-23).

4. Collision dynamics in low energy collisions

4.1. Orbiting effect due to the induced dipole

When an ion with charge q approaches to an atom, the collision dynamics becomes dominated by the ion induced polarization of the target atom. This leads to a mutual attractive polarization force between the collision partners and the trajectory of the incoming ion bends. The effective potential between the collision partners V_{eff} is given by

$$V_{eff} = \frac{b^2}{r^2} E_{cm} - \frac{\alpha q^2}{2r^4}, \qquad (4\text{-}1)$$

where b, r, E_{cm} and α are impact parameter, internuclear distance between the collision partners, collision energy in the center-of-mass system and polarizability of the target atom,

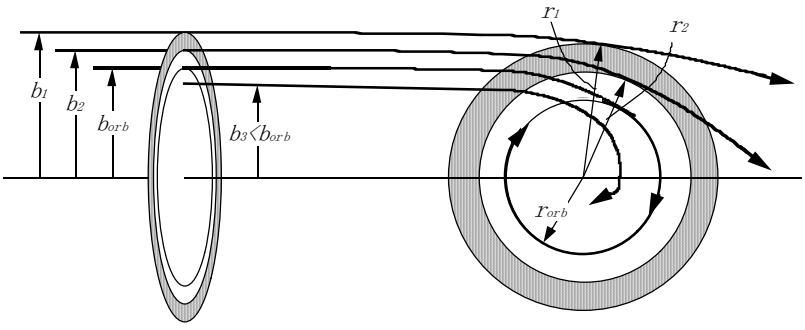

Fig.6. Collision trajectory dominated by induced dipole.

respectively. At a specific impact parameter b_{orb} as a maximum of the effective potential (4-1) just becomes equal to E_{cm}, the collision trajectory puts in an orbit with a radius of r_{orb} round the collision center.

$$b_{orb} = \sqrt{2}\, r_{orb} = \left(\frac{2\alpha q^2}{E_{cm}} \right)^{1/4} \qquad (4\text{-}2)$$

At sufficient low collision energies and sufficient small impact parameters of $b<b_{orb}$, the collision trajectory takes a spiraling orbit towards the collision center. The cross section for such collision is given by

$$\sigma_L = \pi b_{orb}^2 = \pi q \left(\frac{2\alpha}{E_{cm}} \right)^{1/2}. \qquad (4\text{-}3)$$

The cross section of σ_L is well known as "*Langevin cross section*" or "*orbiting cross section*" in inverse proportion to collision velocities [5]. The orbiting radius of r_{orb} increases with decrease of the collision energy. At sufficiently low energies as the orbiting radius of r_{orb} becomes much larger than an interaction range effective for the related reaction in inelastic collisions, the cross section for such reaction can be approximated as

$$\sigma = 2\pi \int_0^{b_{orb}} P(\upsilon, b)\, b db \approx 2\overline{P}\, \pi \int_0^{b_{orb}} b db = \overline{P} \sigma_L, \qquad (4\text{-}4)$$

where $\overline{P}$ is a constant value averaged for a reaction probability P as a function of υ and b. This is the reason why the product of σ and υ is defined as the rate constant. Practically, rate constants measured for various inelastic reactions in the thermal energy region are almost

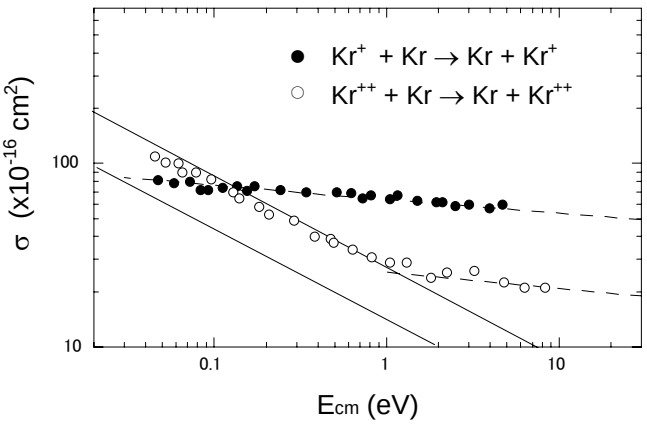

Fig.7. Resonant charge transfer cross sections [6].

constant. Since the Langevin cross section is proportional to the charge state q of projectile ions, it is expected for the charge transfer collisions of multiply charged ions that the energy region where the orbiting effect enhances the charge transfer cross sections at low energies shifts to the higher energy side from near thermal energy region with increasing the charge state q of projectile ions. As seen in Fig.7, resonant double-charge transfer cross sections below 1eV were reproduced by $\sigma_L/2$ and their energy dependence was explained well by the orbiting effect [6].

In the region of $b > b_{orb}$, the relation between an impact parameter b_1 and a closest internuclear distance r_1 is represented by

$$b_1 = r_1\left(1+\frac{\alpha q^2}{2r_1^4 E_{cm}}\right)^{1/2} = r_1\left(1+\frac{r_{orb}^4}{r_1^4}\right)^{1/2}. \qquad (4\text{-}5)$$

Impact parameter ring area between circles with radii of b_1 and b_2 is smaller than that for a corresponding interaction ring between circles with radii of r_1 and r_2 and decreases with decreasing of the collision energy.

$$\pi(b_1^2 - b_2^2) = \pi\left\{r_1^2\left(1+\frac{r_{orb}^4}{r_1^4}\right) - r_2^2\left(1+\frac{r_{orb}^4}{r_2^4}\right)\right\} = \pi(r_1^2 - r_2^2)\left(1-\frac{r_{orb}^4}{r_1^2 r_2^2}\right) \qquad (4\text{-}6)$$

Now it is well known that charge transfer of multiply charged ions in collisions with atomic and molecules takes placed state-selectively at a located inter-nuclear distance. Therefore, the relation between the interaction range effective for the charge transfer and the orbiting radius increasing with decreasing of the collision energy should much affects to the reaction cross section. This analysis predicts that charge transfer cross sections of multiply charged ions have a specific energy dependence which turns from decreasing of (4-6) to increasing of (4-4) with decreasing of the collision energy. Similar energy dependence of charge transfer cross sections can be simulated also in the Ladau-Zener calculation for tentative single curve crossings labeled by ΔE in collisions of $A^{8+} + He \rightarrow A^{7+} + He^{+} + \Delta E$ [7]. Calculated cross sections with and without considering the target polarization are demonstrated for changing ΔE at 2.45eV intervals in Fig.8, The induced dipole clearly enhances cross sections, like to Langevin cross section, at energies lower than near the arrow-marked position where the orbiting radius coincides with the crossing radius.

Energy dependence of cross sections for each crossing labeled by ΔE becomes stronger with increasing of ΔE.

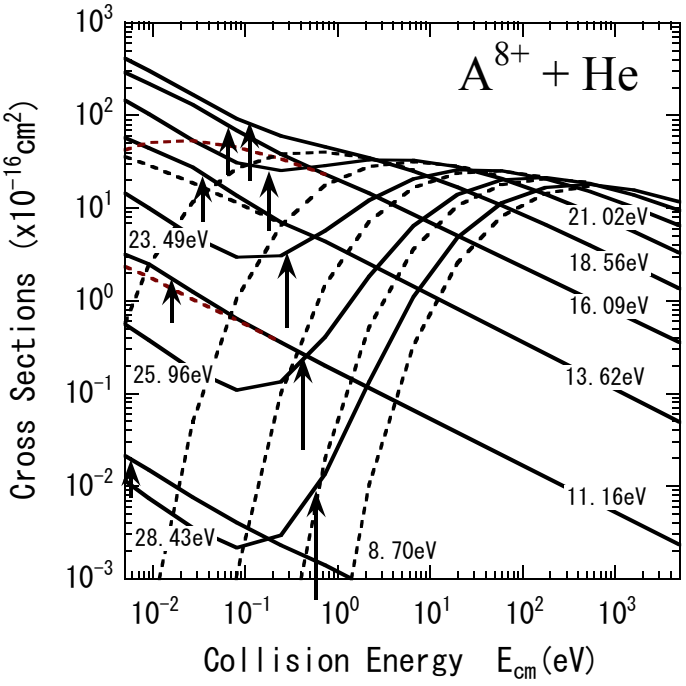

Fig. 8. Landau-Zener calculation for tentative single crossings labeled by ΔE with / without target polarization [7].

5. Classical over barrier model and curve crossing model

Classical over barrier model (COBM) and curve crossing model (CCM) base on the concept of energy matching between initial and final states and both are simple methods very useful to estimate cross sections for the state-selective charge transfer in collisions of multiply charged ions with atoms and molecules.

$$A^{q+} + B \rightarrow A^{(q-1)+}(n) + B^{+} + \Delta E \qquad (5\text{-}1)$$

In the COBM model [8], an electron bound in a n_B state of the target with core charge of Z_B gets over a potential barrier V_m and is captured into a specified n_A state of the projectile ion with core charge of Z_A state-selectively as is illustrated in Fig.9. The first condition for the target electron to get over $V_m = -(Z_A^{1/2} + Z_B^{1/2})^2 / R$ requires the relation (5-2) and the second condition for energy matching between initial and final states gives the relation (5-3).

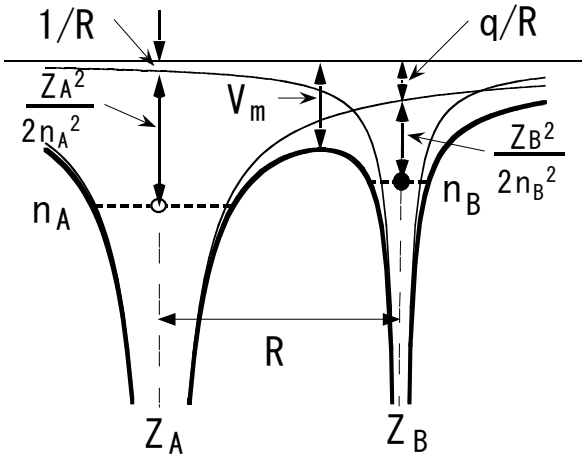

Fig.9. Classical over barrier model [8].

$$I_B + \frac{Z_A}{R} - \frac{(Z_A^{1/2} + Z_B^{1/2})^2}{R} = I_B - \frac{2Z_A^{1/2}Z_B^{1/2} + Z_B}{R} \le 0 \qquad (5\text{-}2)$$

$$I_B + \frac{Z_A}{R} - \left(I_A(n) + \frac{Z_B}{R} \right) = -\Delta E(n) + \frac{Z_A - Z_B}{R_n} = 0 \qquad (5\text{-}3)$$

Here, the reaction energy ΔE is given by the energy difference between ionization potentials of I_A and I_B and equal to $(Z_A\text{-}Z_B)/R$. It means as in the CCM that the charge transfer takes place at $R_n = (Z_A\text{-}Z_B)/\Delta E$ corresponding to a crossing point between potential curves of the initial $(A^{q+}+B)$ state and the final $(A^{(q-1)+}+B^{+})$ state for $Z_A = q$ and $Z_B = 1$ as shown in Fig.10.

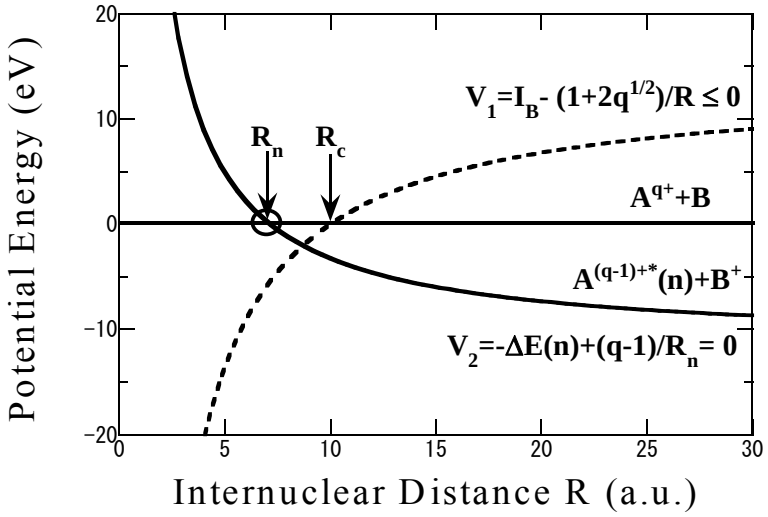

Fig.10. Curve crossing in classical over barrier model

Information concerning the reaction window of the crossing region effective for charge transfer is in need for estimation of the most dominant reaction channel. The relation (5-2) suggests the upper limit R_c of the interaction range for electron transfer as seen in Fig.10. Assuming that energy levels of related ions are of $I=Z^2/2n^2$ in hydrogen like, the quantum number n of excited states which dominantly captures an electron from the target can be estimated by the following relation [8, 9].

$$n \leq \frac{Z_A}{Z_B}\left(\frac{Z_B + 2(Z_A Z_B)^{1/2}}{Z_A + 2(Z_A Z_B)^{1/2}}\right)^{1/2} \qquad (5\text{-}4)$$

In single electron capture processes of multiply charged ions, an electron is captured into higher excited states with increasing the charge state q of projectile ions. Therefore, single electron capture cross sections for highly charged ions with large q can be estimated by $\sigma_n=P\pi R_n^2$ based on the hydrogen like approximation. The cross section of $\sigma_c=\pi R_c^2$ estimated

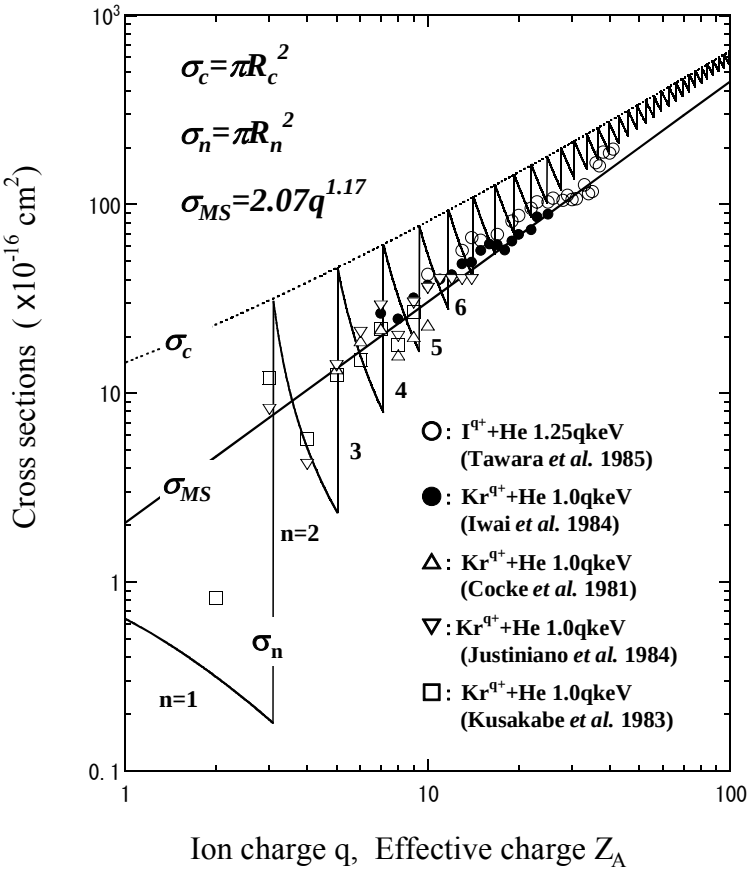

Fig.11. Cross sections for single electron capture of Kr^{q+} and I^{q+} ions in collisions with He as a function of q or effective charge Z_A.

from the relation (5-2) gives the upper limit of single electron capture cross sections.

In Fig.11, cross section data [10, 11, 12, 13, 14] for single electron capture of Kr^{q+} and I^{q+} ions (q=2~41) in collisions with He are shown together with empirical cross section of $\sigma_{MS}=2.07\times10^{-16}\times q^{1.17}$ by Müller & Salzborn [15] as a function of q and they are compared with $\sigma_c=\pi R_c^2$ and $\sigma_n=\pi R_n^2$ in the COBM as a function of effective charge Z_A. As seen in Fig.11, experimental cross section data for single electron capture of low-charged ions, especially $q<8$, strongly depend on q and the prediction of $\sigma_n=\pi R_n^2$ in the COBM fairly well reproduces the oscillating structure in charge dependence. While charge transfer cross sections of multiply charged ions generally have not so strong energy dependence in the keV energy region, it is very interesting what happens in the low energy region.

6. Cross section data for low energy charge transfer of multiply charged ions

The brief outlines of typical characteristics in low energy charge transfer cross section data systematically measured for collision systems listed in Table 1 (b) and (c) will be demonstrated here. Note that project ions in Table 1(b) are produced by a Nier type ion source and these in Table 1 (c) are produced by Mini-EBIS.

6.1. Charge transfer of low-charged rare-gas ions produced by a Nier type ion source

For collision systems listed in Table 1(b) of which projectile ions were produced by a Nier type ion source, electron capture cross sections of low-charged rare-gas ions were measured. Previously it was proved experimentally by drift tube technique that the symmetric resonant double charge transfer cross sections in Kr^{2+}/Kr and Xe^{2+}/Xe systems are enhanced in according with a half of the Langevin cross section at low energies where the collision is dominated by an attractive potential of an induced dipole [6, 16]. In symmetric collision systems of Ar^{2+}/Ar, Ar^{3+}/Ar, Kr^{2+}/Kr and Kr^{3+}/Kr, total attenuation cross sections of project ions in their own gases increased gradually with decreasing the collision energy and partial charge transfer cross sections strongly depended on the collision energy [1, 2]. The remnants of the attenuation cross section subtracted by partial charge transfer cross sections almost agreed with a half of Langevin cross section in eq.(4-3) at low energies. Experimental facts suggest that the symmetric resonant charge transfer process of $A^{q+} + A \rightarrow A + A^{q+}$ becomes most dominant not only for q=2 but also for q=3 at energies as low as the collision is dominated by an attractive potential of an induced dipole.

Generally, doubly charged rare gas ions produced in a conventional electron impact type ion source such as a Nier type ion source usually are accompanied with low-lying

metastable ions in states of $^1D_2$ and $^1S_0$ added to the ground state ions in $^3P_{1/2,3/2}$. Practically, single charge changing cross section of σ_{21} for collision systems of Ar^{2+}/He and Kr^{2+}/He except for Ne^{2+}/He strongly depend on the electron impact energy. Changing the electron impact energy, partial cross sections of $\sigma_{21}(^1D_2)$ and $\sigma_{21}(^3P)$ in Ar^{2+}/He system and of $\sigma_{21}(^1S_0)$ and $\sigma_{21}(^1D_2)$ in Kr^{2+}/He are estimated. It is interesting that the collision system of Ne^{2+}/He has not only no evidence for long-living excited ions existing but also a very steep threshold structure of σ_{21} near $E_{cm}\approx16$ eV as seen in Fig.12. The reason why cross section data for the Ne^{2+}/He system is quite different from others remains unresolved.

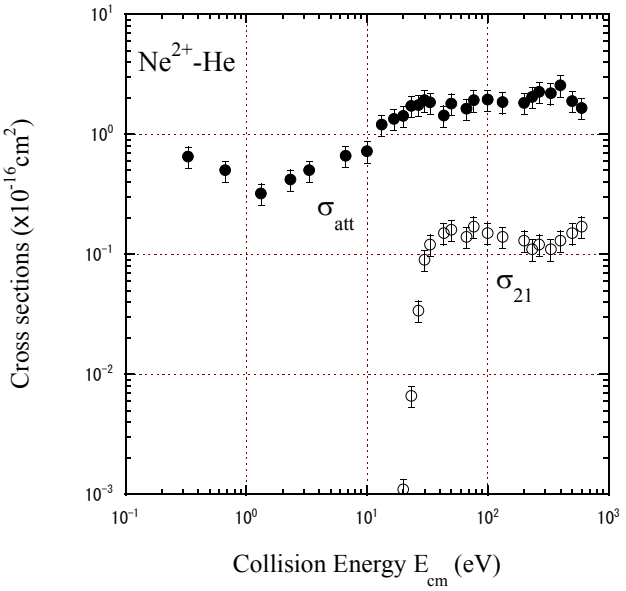

Fig.12. Cross sections of σ_{att} and σ_{21} in Ne^{2+}/He collision systems.

6.2. Charge changing cross sections of multiply charged ions produced by the Mini-EBIS

The contamination of long-living excited ions often causes significant and dramatic effects on the observed cross sections. Min-EBIS is operated at ultra high vacuum in order of 10^{-9} Pa. At such low densities, there is little probability of metastable production via electron capture collisions and, even if metastable ions are produced, they will be quenched during long confinement times in the DC ion-extraction mode. Practically no existence of long-living excited ions was found in multiply charged ion beams extracted from the Mini-EBIS except for C^{2+} and O^{2+} beams. Charge changing cross sections of multiply charged ions in collision systems listed in Table 1 (c) were systematically measured in the low energy range of 0.5 to 2000 eV per ion charge q. Some of them were already reported in [17] for He^{2+}/He and He^{2+}/H_2, in [22] for He^{2+}/CO, N_2 and O_2, and Kr^{q+}/Ne, N_2, O_2 and CO (q=7-9), in [4] for C^{4+}, N^{4+} and O^{4+}/He, in [23] for C^{4+}/Ar and $C_nH_{2(n+1)}$ (n=1~4), in [24] for C^{4+}/H_2, N_2 and O_2, in

[25] for Ar^{q+}/H_2 (q=6-9,11), in [7] for Ar^{q+}/He (q=6-9,11) and I^{q+}/He (q=24-26), in [26] for Ar^{q+}/Ne, in [27] for C^{q+}/He and H_2 (q=2-5) and in [27, 28] for C^{q+}, N^{q+} and O^{q+}/He (q=2~6), respectively. As well known, charge transfer processes of multiply charged ions frequently are followed a transfer ionization, in which case ions release a part of electrons captured from target. Note that, in the present measurements, product ions are identified by the final charge state and contributions from the transfer ionization are mixed. Here, the brief outlines of characteristic cross section data for low energy charge changing collisions of multiply charged ions with atoms and molecules will are introduced.

6.2.1. Importance of double electron capture in low energy He^{2+} collisions

In symmetric collision system of He^{2+}-He, it is expected that the symmetric resonant double electron transfer is dominant and its cross section is enhanced at very low energies due to the orbiting effects. In a series of low energy cross section measurements, both beam attenuation cross sections σ_{att} and single-charge changing cross sections σ_{21} were measured for collisions of He^{2+} ions with He, H_2, N_2 and CO and the upper limits for double-charge changing cross section σ_{20} are estimated by the difference σ_{att}-σ_{21} [17, 22]. With decreasing the collision energy, σ_{21} decreased but total attenuation cross sections σ_{att} increased oppositely in every collision systems. The estimated σ_{20} informs that double electron capture processes become predominant in low energy collisions of He^{2+} ions.

Charge transfer cross section data for the He^{2+}-H_2 collision system are summarized in Fig.13. Open and solid marks indicate single- and double-electron capture cross sections of σ_{21} and σ_{20}, respectively. The whole picture about relation between the single-electron transfer and the double-electron transfer in the wide energy range has been revealed by the present data.[17].

$$He^{2+} + H_2 \rightarrow He^{+}(2l) + H_2^{+} \qquad (6\text{-}1)$$

$$\rightarrow He^{*}(1s2l) + (H_2)^{2+} \qquad (6\text{-}2)$$

$$\rightarrow He^{*}(1s3l) + (H_2)^{2+} \qquad (6\text{-}3)$$

Hoekstra et al. reported that emission cross sections for HeII(2p→1s) in process (6-1) [20] and those for HeI($1s2p\rightarrow1s^2$) in processes (6-2) and (6-3) [21]. Their data support that the dominant reaction channel changes drastically from the single electron capture process to the double electron capture process with decreasing the collision energy. Theoretical calculation

by Shimakura et al. [19] also predicts predominance of the double electron capture process in the low energy region. In the double electron capture collisions of He^{2+} with H_2, product $(H_2)^{2+}$ ions soon dissociate to two protons carrying kinetic energy of approximately 9 eV due to Coulomb explosion even though very low energy collisions. Such process should take place with a very large cross section at very low energies. This is great importance, for example as a proton acceleration mechanisms in interstellar clouds and high temperature plasmas.

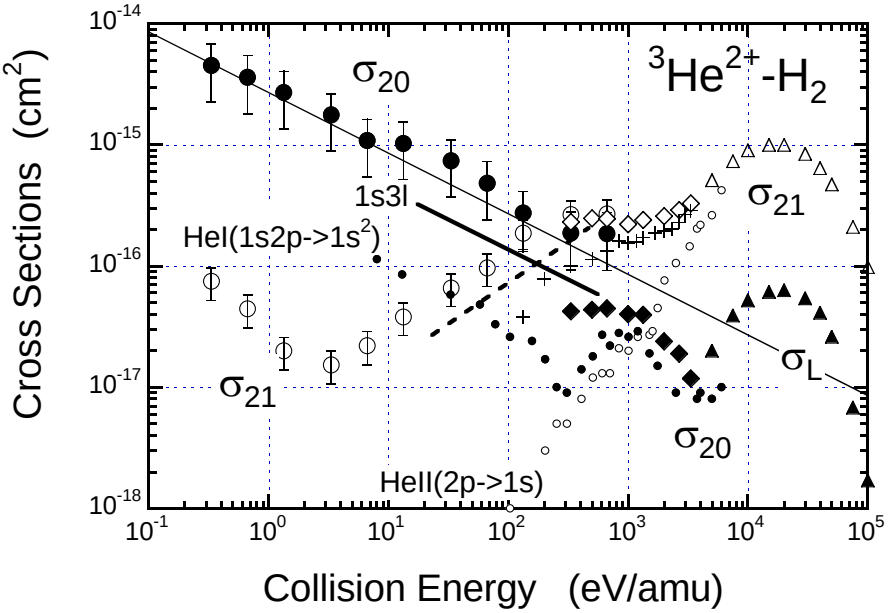

Fig.13. Single- and double-charge changing cross sections of He^{2+} with H_2.
●○:Okuno [17], ◆◇:Kusakabe [18],—--:Shimakura [19], ●○:Hoekstra [20, 21].

6.2.2. Charge changing cross sections of C^{q+}, N^{q+} and O^{q+} in collisions with He and H_2.

Charge changing cross sections of C^{q+}, N^{q+} and O^{q+} incident on He and H_2 were measured systematically for q=2~6 at low energies below 1 keV/amu [28]. Cross section data for q=5 and 6 are typically demonstrated in Figs.14 and 15 for He and H_2 targets, respectively. As seen in Fig.14, single- and double-charge changing cross sections for collision systems of C^{q+}, N^{q+} and O^{q+} ions with He almost uniquely depends on the incident charge q but not on the projectile species. These characteristics can be understood from relation between potential curves for initial and final channels in charge transfer collisions. As shown in Fig.16, an arrangement of potential curves for electron capture channels is very similar for C^{q+}, N^{q+} and O^{q+}-He systems with same incident charges q and crossing positions between initial and final potential curves drastically changes when the incident charge q changes. Inner crossing leads to strong collision energy dependence on cross sections. However, in collision systems of C^{q+}, N^{q+} and O^{q+}-H_2, the strong dependence on the incident charge and the collision energy as seen

in He targets dose not appear as shown in Fig.15. Molecules have freedoms of vibration and rotation and their ionic energy levels are in band likes which is different from discrete atomic energy levels. In the collision system with molecular targets, an incident channel can easily make energy matching with final charge transfer channels including various molecular ionic excitations. In collisions of C^{q+}, N^{q+} and O^{q+} ions with H_2, single charge changing cross sections are irrespective to the incident charges and the projectile species and take a similar energy dependence where increases of decreases gently with decreasing the collision energy and becomes to be in inverse proportion to the collision velocity at sufficiently low energies. The energy dependence for case of H_2 targets is quite different from those for case of He targets.

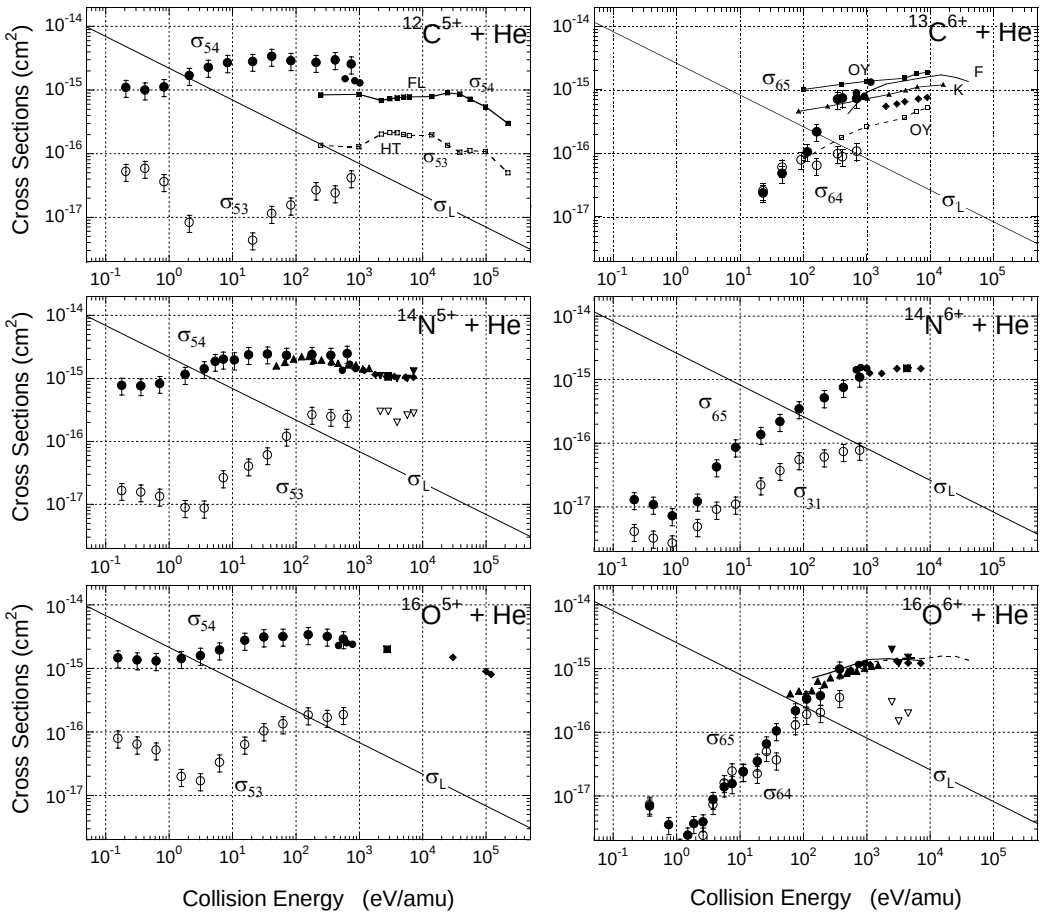

Fig.14. Charge changing cross sections of $C^{5+,\,6+}$, $N^{5+,\,6+}$ and $O^{5+,\,6+}$ incident on He [28].

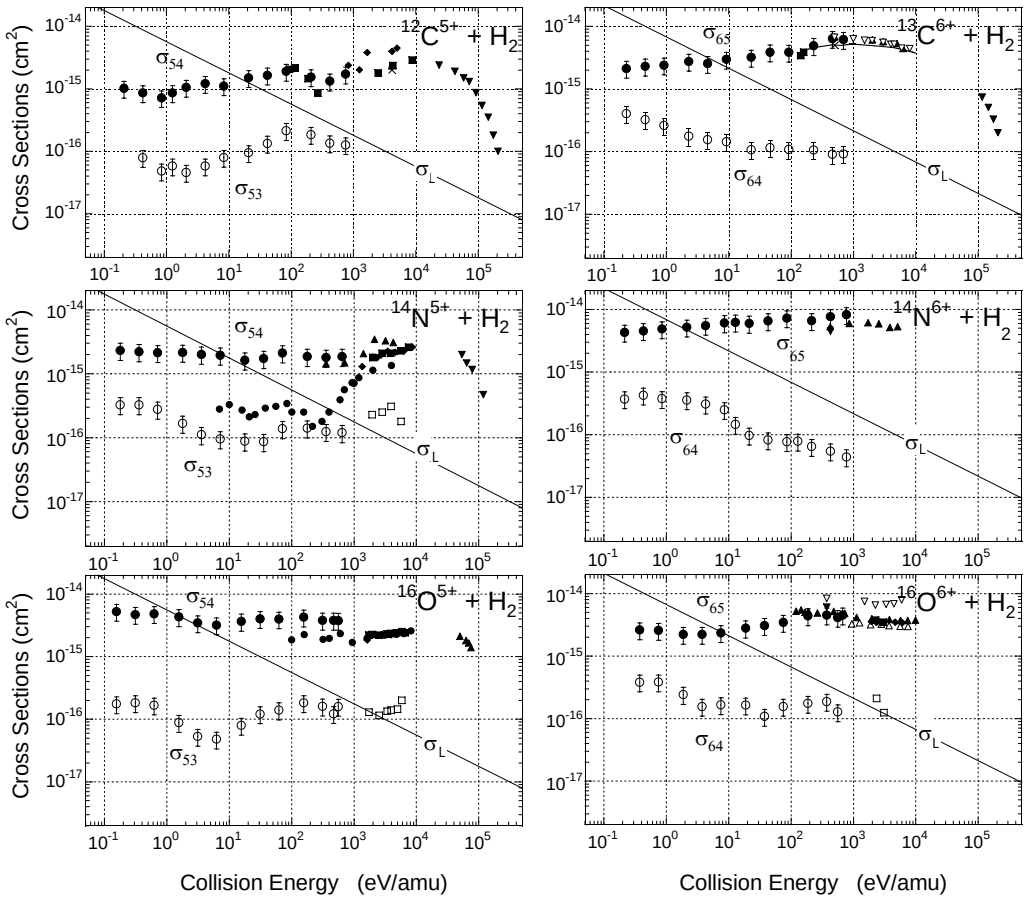

Fig.15. Charge changing cross sections of $C^{5+,\,6+}$, $N^{5+,\,6+}$ and $O^{5+,\,6+}$ incident on H_2

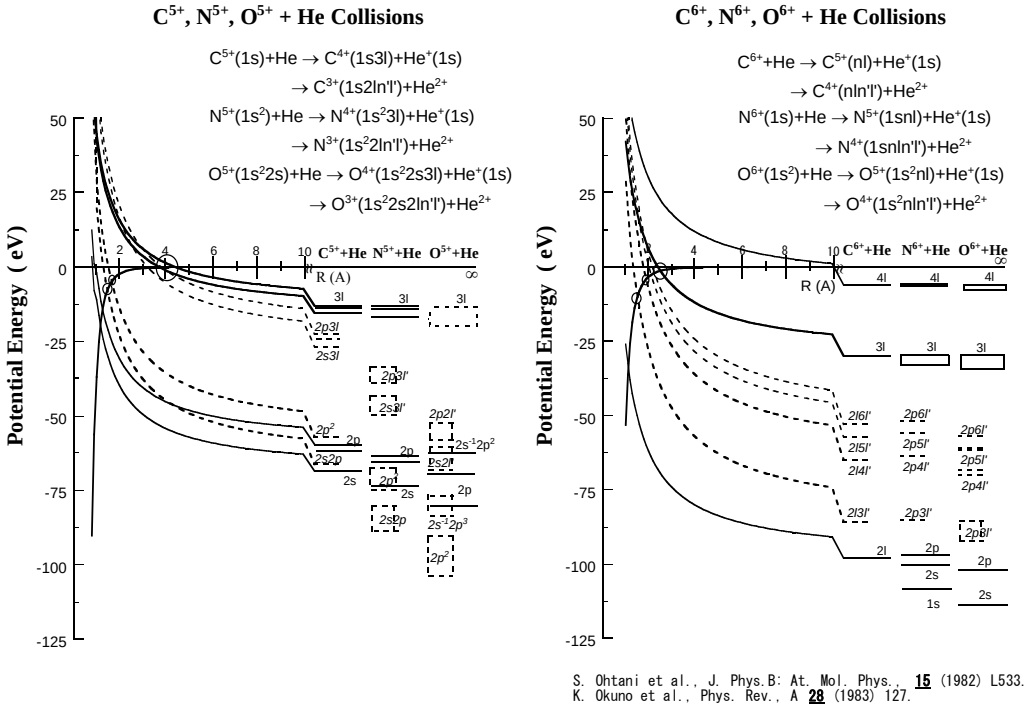

Fig. 16. Potential curves for electron capture collisions of C^{q+}, N^{q+} and O^{q+} (q=5, 6) ions with He.

6.2.3. Charge changing cross sections of Ar^{q+} (q=6~9, 11) incident on H_2 and He.

The cross section data of single- and double-charge changing collisions of Ar^{q+} (q=6~9, 11) with the two electron targets H_2 and He have been measured systematically in the low energy range 0.5 to 2000 eV per ion charge [7, 25].

In Fig.17, measured cross sections are summarized together with previous experimental and theoretical data. Single-charge changing cross sections gradually increase with decreasing

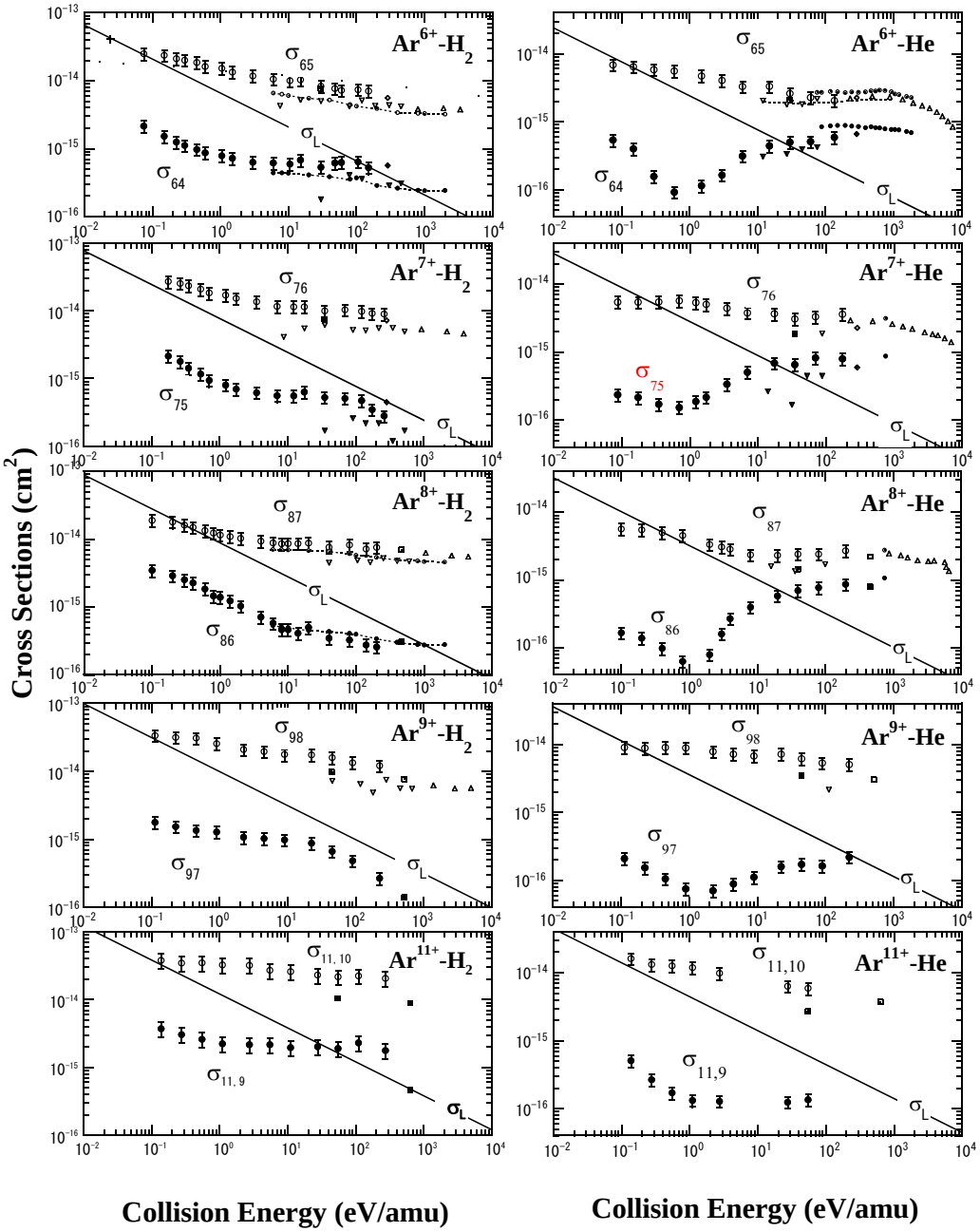

Fig.17. Single- and double-charge changing cross sections of Ar^{q+} (q=6~9, 11) incident on H_2 and He.

the collision energy and they almost converges to the Langevin cross section σ_L at the low energy end. Double-charge changing cross sections also increase along σ_L in lower energies. The single-charge changing cross sections for the H_2 targets are almost three times as large as those for the He targets and their ratio of $\sigma(He)/\sigma(H_2)$ is close to $[IP(He)/IP(H_2)]^{-2.72}$ predicted by the scaling law [15]. On the other hands, the double-charge changing cross sections are smaller than one tenth of the single-charge changing cross section and strongly depend on the collision energy in contrast to the single-charge changing cross section and also increase at lower energies. In the low energy collisions, the collision dynamics drastically changes giving rise to various new effects and interesting phenomena. The Coulomb electric field created by the ionic charge polarizes neutral targets and an ion-induced dipole leads to a mutual attraction between the collision partners. The induced dipole interaction can capture the ion in a spiral trajectory close to the collision center at sufficiently small impact parameters and the trajectory takes a circular orbit around the target at an appropriate impact parameter [5]. At sufficiently low collision energies where the collision is dominated by the ion-induced dipole, the orbiting cross section is enlarged in inverse proportion to the collision velocity. In various thermal reactions of singly charged ions, almost all reaction rates are constant. This signature is well known as the orbiting effects due to the ion-induced dipole interaction. As the incident ion charge q becomes large, it is expected instinctively that the enhancement of cross section due to the orbiting effects can be observed at energies far much higher than thermal energy. Practically, such expectation has been never realized on single electron capture cross sections measured for Ar^{q+}-H_2, He (q=6~9, 11) and I^{q+}-He (q=24~26) [7]. Taking simple models into consideration, we can know that not only the Langevin cross section σ_L in relation (4-3) but also the empirical single electron capture cross section σ_{MS} by [15] similarly increase almost in proportion to the ionic charge q, therefore, the boundary energy for the orbiting effects appearing almost stays at near 0.1 eV/amu even when q becomes large. On the other hands, double-charge changing cross sections are strongly dependent on the collision energy and also increase again at low energies as seen in Fig.17.

6.2.4. Charge changing cross sections of multiply charged ions incident on many electron targets.

Charge changing cross sections for Ar^{q+} (q=4~9) incident on Ne [26], Kr^{q+} (q=4~9) incident on CO, Kr^{q+} (q=7~9) incident on Ne, and Kr^{8+} incident on N_2 and O_2 [22] were measured in a series of cross section measurements. Usually, charge changing processes of multiply charged ions for many electron targets are very complicate, as many electron capture

are followed by transfer ionization and target fragmentation. The charge changing cross sections depend on the incident charge q, but are not so sensitive to the molecular target species. In Fig.18, multiple-charge changing cross sections of up to fourfold charge change for Kr^{8+} incident on atomic target Ne and up to fivefold charge change for Kr^{8+} incident on molecular targets of N_2, CO and O_2 are demonstrated. As seen in Fig.18, measured cross sections for many electron targets of N_2, CO and O_2 are very similar each others both in magnitude and energy dependence, and they are larger than those for atomic target of Ne. The energy dependence of single-charge changing cross sections is not so strong commonly for every system but those of multiple-charge changing cross sections become stronger and show a deeper minimum as the degree of charge change becomes higher. The band-like distribution of ionic energy levels for molecular targets seems to lead to insensitivity for molecular target species and larger cross sections than that for Ne target. The strong energy dependence observed in multiple-charge changing cross sections should be determined by the competition between the orbiting radius and the effective interaction range for the related reaction. Thus, at low energies general scaling laws and simple model assuming linear trajectory do not seem to apply.

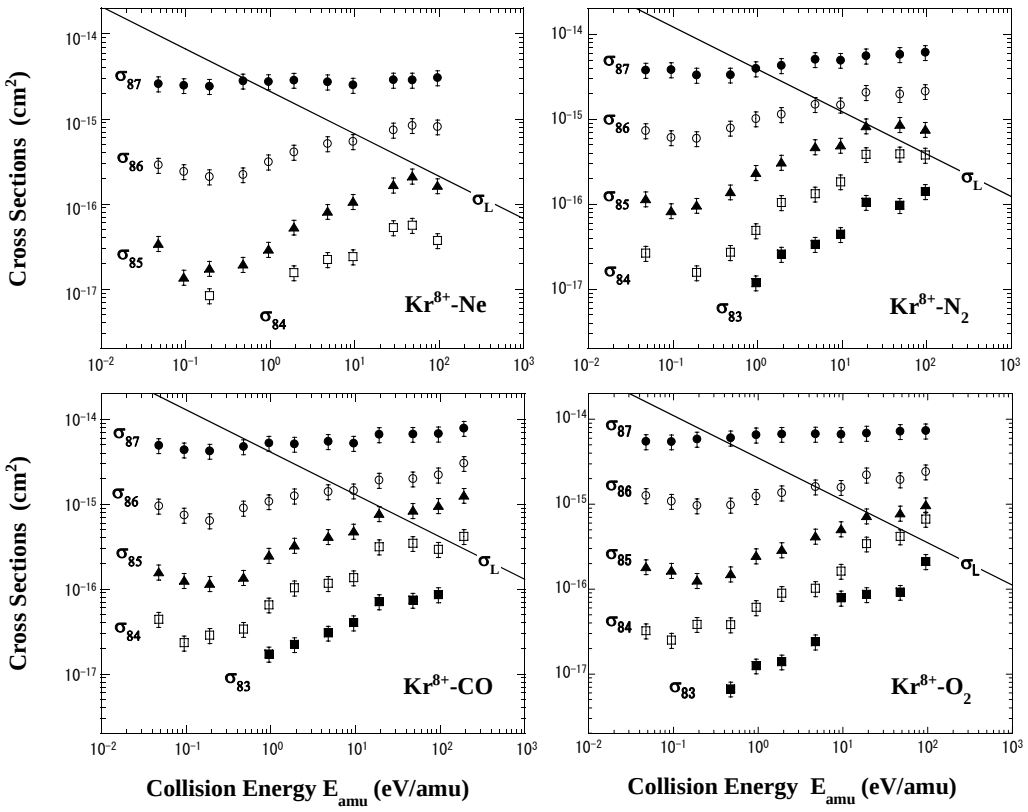

Fig.18. Charge changing cross sections of Kr^{8+} incident on Ne, N_2, CO and O_2.

In slow collisions of He^{2+} and Kr^{8+} highly charged ions with H_2, N_2, O_2 and CO, multiple-charge changing charge processes have been investigated by a new triple coincidence technique for three particle detection using twin OPIG systems and complicated reaction processes accompanied with fragmentation have been revealed [29]. For example, single-, double-, triple- and quadruple-charge changing processes in collisions of Kr^{8+} with N_2 are resolved as follows.

$$Kr^{8+} + N_2 \rightarrow Kr^{7+} + N_2^{+} \quad (6\text{-}4)$$

$$\rightarrow Kr^{7+} + N_2^{2+} + e^{-} \quad (6\text{-}5)$$

$$\rightarrow Kr^{7+} + N^{+} + N^{+} + e^{-} \quad (6\text{-}6)$$

$$\rightarrow Kr^{7+} + N^{2+} + N^{+} + 2e^{-} \quad (6\text{-}7)$$

$$Kr^{8+} + N_2 \rightarrow Kr^{6+} + N^{+} + N^{+} \quad (6\text{-}8)$$

$$\rightarrow Kr^{6+} + N^{2+} + N \quad (6\text{-}9)$$

$$\rightarrow Kr^{6+} + N^{2+} + N^{+} + e^{-} \quad (6\text{-}10)$$

$$\rightarrow Kr^{6+} + N^{2+} + N^{2+} + 2e^{-} \quad (6\text{-}11)$$

$$\rightarrow Kr^{6+} + N^{3+} + N^{+} + 2e^{-} \quad (6\text{-}12)$$

$$\rightarrow Kr^{6+} + N^{3+} + N^{2+} + 3e^{-} \quad (6\text{-}13)$$

$$Kr^{8+} + N_2 \rightarrow Kr^{5+} + N^{2+} + N \quad (6\text{-}14)$$

$$\rightarrow Kr^{5+} + N^{3+} + N^{+} + e^{-} \quad (6\text{-}15)$$

$$\rightarrow Kr^{5+} + N^{2+} + N^{2+} + e^{-} \quad (6\text{-}16)$$

$$\rightarrow Kr^{5+} + N^{3+} + N^{2+} + 2e^{-} \quad (6\text{-}17)$$

$$\rightarrow Kr^{5+} + N^{3+} + N^{3+} + 3e^{-} \quad (6\text{-}18)$$

$$Kr^{8+} + N_2 \rightarrow Kr^{4+} + N^{3+} + N \quad (6\text{-}19)$$

$$\rightarrow Kr^{4+} + N^{2+} + N^{2+} \quad (6\text{-}20)$$

$$\rightarrow Kr^{4+} + N^{3+} + N^{2+} + e^{-} \quad (6\text{-}21)$$

$$\rightarrow Kr^{4+} + N^{3+} + N^{3+} + 2e^{-} \quad (6\text{-}22)$$

By the multi-coincidence technique using twin OPIG systems, some new phenomena relevant to collision dynamics and oriented fragmentation also have been found at low energies. To understand in detail reaction mechanisms in low energy collisions of multiply charged ions with atoms and molecules yet more theoretical and experimental investigations on collision dynamics at low energies are required.

Acknowledgement

The present cross section measurements were carried out over twenty four years in collaboration with many colleagues and many students. The author wishes to express his sincere acknowledgement to all members of collaborators and also his thanks to staffs of NIFS Atomic and Molecular Data Research Center for inputting accumulated data into the NIFS database system. This work was carried out under the collaborating research program at National Institute for Fusion Science (NIFS06KYAM010).

References

[1] K. Okuno, J. Physics. Soc. Jpn., **55** (1986) 1504.

[2] K. Okuno and Y. Kaneko, Mass Spectroscopy, **34** (1986) 351.

[3] K. Okuno, Jpn. J. Appl. Phys., **28** (1989) 1124.

[4] K. Okuno K. Soejima and Y. Kaneko, Nucl. Inst. Meth. Phys. Res., **B53** (1991) 387.

[5] G. Gioumousis and D. P. Stevenson , J. Chem. Phys., **29** (1958) 294.

[6] K. Okuno, T. Koizumi and Y. Kaneko, Phys. Rev. Letters, **40** (1978) 1708.

[7] K. Okuno, H. Saitoh, K. Soejima, S. Kravis and N. Kobayashi, *The Physics of Electronic and Atomic Collisions, ed. By L. J. Dubé et al.,* AIP Conference proceedings, **360** (1995) 867.

[8] H. Ryufuku, K. Sasaki and T. Watanabe, Phys. Rev., A **21** (1980) 745.

[9] T. Iwai, Y. Kaneko, M. Kimura, N. Kobayashi, A. Matsumoto, S. Ohtani, K. Okuno, S. Takagi, H. Tawara and S. Tsurubuchi, Phys. Rev., **A 26** (1982) 105.

[10] H. Tawara, T. Iwai, Y. Kaneko, M. Kimura, N. Kobayashi, A. Matsumoto, S. Ohtani, K. Okuno, S. Takagi and S. Tsurubuchi, J. Phys. B: At. Mol. Phys., **18**, (1985) 337.

[11] T. Iwai, Y. Kaneko, M. Kimura, N. Kobayashi, A. Matsumoto, S. Ohtani, K. Okuno, S. Takagi, H. Tawara and S. Tsurubuchi, J. Phys. B: At. Mol. Phys., **1** (1985) L95.

[12] C. L. Cocke, R. DuBois, J. T. Gray and E. Justiniano, IEEE Trans. Nucl. Sci., **NS-28** (1981) 1032.

[13] E. Justiniano, C. L. Cocke, R. DuBois, J. T. Gray, C. Can and W. Waggoner, Phys. Rev.,

A 29 (1984) 1088.

[14] T. Kusakabe, H. Hanaki, N. Nagai, T. Horiguchi, I. Konomi and M. Sakisaka, Phys. Scr., **T3** (1983) 191.

[15] A. Müller and E. Salzborn, Phys. Letter, **62A** (1977) 391.

[16] T. Koizumi, K. Okuno and Y. Kaneko, J. Phys. Soc. Japan, **51** (1982) 2750.

[17] K. Okuno, K. Soejima and Y. Kaneko, J. Phys. B: At Mol. Opt. Phys., **25** (1992) L105.

[18] T. Kusakabe, Y. Yoneda, Y. Mizumoto and K. Katsurayama, J. Phys. Soc. Japan, **59** (1990)1218.

[19] N. Shimakura, M. Kimura and N. F. Lane, Phys. Rev., A **47** (1993)709.

[20] R. Hoekstra, A. R. Schlatmann, F. J. de Heer and R. J. Morgenstern, J. Phys. B: At. Mol. Opt. Phys., **22** (1989)L603.

[21] R. Hoekstra, H. O. Folkerts, J. P. M. Beijers, R. Morgenstern and F. J. de Heer, J. Phys. B: At. Mol. Opt. Phys., **27** (1994)2021.

[22] K. Ishii, K. Okuno and N. Kobayashi, Physica Scripta, **T80** (1999) 176.

[23] K. Soejima, K. Okuno and Y. Kaneko, Org. Mass Spectrometry, **28** (1993) 344.

[24] K. Soejima, C. J. Latimmer, K. Okuno and N. Kobayashi and Y. Kaneko, J. Phys. B: At. Mol. Opt. Phys., **25** (1992) 3009.

[25] S. Kravis, H. Saitoh, K. Okuno, K. Soejima, M. Kimura, I. Shimamura, Y. Awaya, Y. Kaneko, M. Oura and N. Shimakura, Phys. Rev., **A52** (1995) 1206.

[26] K. Suzuki, K. Okuno and N. Kobayashi, Physica Scripta, **T73** (1997) 172.

[27] K. Ishii, T. Tanabe, R. Lomsdze and K. Okuno, Physica Scripta, **T92** (2001) 332.

[28] K. Ishii, A. Itoh and K. Okuno, Phys. Rev., **A70** (2004) 042716.

[29] T. Kaneyasu, T. Azuma and K. Okuno, J. Phys. B: At. Mol. Opt. Phys., **38** (2005) 1341.